Scripta Materialia 157 (2018) 90–94

Contents lists available at ScienceDirect

Scripta Materialia

journal homepage: www.elsevier.com/locate/scriptamat

Regular article

Mechanical softening of thermoelectric semiconductor Mg_2Si from nanotwinning

Guodong Li [a,b,*], Qi An [c], Sergey I. Morozov [d], Bo Duan [a], William A. Goddard III [e], Pengcheng Zhai [a], Qingjie Zhang [a], G. Jeffrey Snyder [b,**]

[a] State Key Laboratory of Advanced Technology for Materials Synthesis and Processing, Wuhan University of Technology, Wuhan 430070, China
[b] Department of Materials Science and Engineering, Northwestern University, Evanston, IL 60208, USA
[c] Department of Chemical and Materials Engineering, University of Nevada Reno, Reno, Nevada 89557, USA
[d] Department of Computer Simulation and Nanotechnology, South Ural State University, Chelyabinsk 454080, Russia
[e] Materials and Process Simulation Center, California Institute of Technology, Pasadena, California 91125, USA

ARTICLE INFO

Article history:
Received 24 April 2018
Received in revised form 13 July 2018
Accepted 1 August 2018
Available online 9 August 2018

Keywords:
Nanotwin-induced softening
Structure - property relation
Thermoelectric material Mg_2Si
ab-initio calculation

ABSTRACT

Nanotwinning exhibits strengthening effects in many metals, semiconductors, and ceramics. However, we show from *ab-initio* calculations that nanotwins significantly decrease the strength of thermoelectric semiconductor Mg_2Si. The theoretical shear strength of nanotwinned Mg_2Si is found to be 0.93 GPa, much lower than that (6.88 GPa) of flawless Mg_2Si. Stretching the Mg—Si bond under deformation leads to the structural softening and failure of flawless Mg_2Si. While in nanotwinned Mg_2Si, the Mg—Si bond at the twin boundary (TB) is expanded to accommodate the structural misfit, weakening the TB rigidity and leading to the low ideal shear strength.

Solid-state thermoelectric (TE) technology, which can realize the direct conversion from heat to electrical energy, attracts renewable attention recently because it could play an essential role in relieving the global energy crisis [1,2]. Mg_2Si based TE material is a promising high-performance candidate with the *zT* value of 1.5 in the mediate temperature range [3–7]. Therefore, Mg_2Si, which consists of globally abundant and eco-friendly elements, is now being considered for application in the automobile waste heat recovery system [8]. However, under thermal cycling loads, thermo-mechanical stress easily causes the crack initiation of Mg_2Si, hence leading to the mechanical failure of Mg_2Si TE devices. Thus, mechanical properties of Mg_2Si are of vital significance for its engineering applications.

The roles of nanotwins on mechanical properties of metal, semiconductor, and ceramics have been widely examined. In particular, nanoscale twins were found very efficient to strengthening the materials. Lu et al. synthesized stable nanotwinned copper samples with a high twin density, which exhibit a ten times higher tensile strength compared to traditional coarse-grained copper [9]. An. et al. showed from quantum mechanics (QM) simulations that the ideal shear strength of boron carbide can be enhanced by 11% when inserting nanotwins [10]. Huang. et al. directly synthesized highly twinned diamond samples with an average grain size of ~5 nm, which exhibit unprecedented high hardness (Vickers hardness of ~200 GPa) and high thermal stability [11]. Tian et al. reported that nanotwinned cubic boron nitrides possess an extremely high Vickers hardness (>100 GPa) and a large fracture toughness (>12 MPa $m^{1/2}$) [12]. Our previous *ab-initio* study showed that through introducing nanoscale twin boundaries, the ideal shear strength of TE semiconductor Bi_2Te_3 and InSb can be enhanced by 215% and 11%, respectively [13,14]. A recent experiment by Jang et al. showed the formation of nanotwins in TE semiconductor Mg_2Si [15], suggesting that they may play an important role in the mechanical properties. However, this remains unexplored.

To understand how nanotwins influence the mechanical properties of Mg_2Si, we utilized *ab-initio* calculations at the Perdew-Burke-Ernzerhof (PBE) functional level to examine the theoretical strength and failure mechanism under pure shear and biaxial shear deformations, respectively. We find that the theoretical shear strength of nanotwinned Mg_2Si is only 0.93 GPa which is much lower than that (6.88 GPa) of flawless Mg_2Si. This is in contrast with the above examples that the strength of materials is enhanced by nanotwins. This nanotwin-induced softening behavior in Mg_2Si arises from the expanded and weakened Mg—Si bond in the twin boundary (TB). We also find that

* Corresponding author at: State Key Laboratory of Advanced Technology for Materials Synthesis and Processing, Wuhan University of Technology, Wuhan 430070, China.
** Corresponding author.
E-mail addresses: guodonglee@whut.edu.cn (G. Li), jeff.snyder@northwestern.edu (G. Jeffrey Snyder).

https://doi.org/10.1016/j.scriptamat.2018.08.002
1359-6462/

compression plays an essential role in determining the theoretical strength of flawless Mg_2Si under biaxial shear load. But it has little influence on strength and deformation mode of nanotwinned Mg_2Si.

All *ab-initio* calculations were implemented in the VASP software [16,17], employing the PBE functional and the projector augmented wave (PAW) potentials to account for the core-valence interactions [18,19]. A kinetic energy cutoff of 500 eV was used for geometry optimization. The electronic self-consistent and force convergence criterion are 1×10^{-6} eV and 1×10^{-2} eV/Å, respectively. The Monkhorst-Pack centered *k*-points sampling with a fine resolution of $2\pi \times 1/40$ Å^{-1} was performed for all calculations. The pure shear and biaxial shear simulation setups are similar with our previous studies on other important TE semiconductors [20–22], which is explained in the Supplementary Material (SM).

Previous theoretical study showed that (1-1-1)[-11-2] is the least stress slip system for Mg_2Si [23], suggesting that the most plausible slip plane for Mg_2Si is the {1-1-1} plane. Thus, the nanotwinned Mg_2Si was constructed using the {1-1-1} plane as the twin plane, and the nanotwinned model was sheared along twin plane to investigate the role of TB on the mechanical properties. This nanotwinned structure was observed experimentally, suggesting it can be stably formed [15]. We considered the TB plane made of Si atoms, as observed in previous experiments [15]. The TB might be formed by Mg atoms, but this situation will not be considered in this paper since no experimental evidences have shown the existence of this type of TB. For comparison, we investigated the shear deformation of single crystal Mg_2Si along the most plausible slip system (1-1-1)[-11-2] and its opposite slip system (1-1-1)[1–12]. In the initial nanotwinned Mg_2Si (Fig. S2(a)) [15], the pre-stress might exist in the nanotwinned structure. However, structural relaxation allows the local atomic movement at the twin boundary (TB) to release the pre-stress. Thus, the relaxed structure (Fig. S2(b)) is stress-free, which is adopted for the shear simulations. In addition, the neighbor structure at the TB remains ideal structural symmetry, suggesting the initial TB structure can maintain perfect TB interface after relaxation, as shown in Fig. S3 in the SM.

We first investigate the shear responses of nanotwinned Mg_2Si under pure shear deformation, as shown in Fig. 1. We predicted an elastic moduli of 23.8 GPa for nanotwinned Mg_2Si from the slope of stress-strain relations at small strains (Fig. 1(a)). Under pure shear load, the theoretical shear strength of the nanotwinned Mg_2Si is found to be 0.93 GPa at the shear strain of 0.05. For single crystal Mg_2Si, the predicted elastic moduli is 46.4 GPa, which is twice higher than that (23.8 GPa) of its nanotwinned structure. The local atomic rearrangement in the nanotwinned structure leads to the enlarged Mg—Si bond length (2.88 Å) at the TB compared with that (2.75 Å) in the single crystal Mg_2Si (Fig. S2). This gives rise to a more weakened TB rigidity compared with that of the Mg—Si framework in the single crystal Mg_2Si. Thus, the TB structure is much weaker in resisting the shear deformation compared with flawless Mg_2Si, leading to a much lower elastic modulus of nanotwinned structure than the flawless Mg_2Si. In addition, we calculated the elastic constant matrix of single crystal and nanotwinned Mg_2Si, and then estimated the shear modulus (G) using the Voigt-Reuss-Hill method [24]. We found that the shear modulus of nanotwinned structure is 32.4 GPa, which is much lower than that (50.6 GPa) of single crystal Mg_2Si. This is another evidence showing that the elastic modulus decreases with nanotwinning. The ideal shear strength of Mg_2Si along (1-1-1)[-11-2] is 6.88 GPa, which is lower than that (8.63 GPa) along its opposite direction (1-1-1)[-11-2]. But it is much higher than that (0.93 GPa) of the nanotwinned model, indicating that nanotwining significantly softens Mg_2Si. The twin softening effects was also observed in boron rich boron carbide ($B_{13}C_2$) [25].

To examine shear stress changes along different directions during shearing, we extracted the stress tensor of nanotwinned Mg_2Si during pure shear process, as shown in Fig. S4. After relaxation (at 0.0 shear strain), all the shear stress is zero, indicating the nanotwinned Mg_2Si is a stress-free cell. The maximum residual stress is $\sigma_{yy} = -0.069$ GPa at 0.071 shear strain, which is much less than the value (0.1 GPa) of our convergence criterion on residual stress. Fig. S4 clearly shows that the residual stress along other five directions is negligible.

Under biaxial shear (compression + shear) load, the theoretical strength of nanotwinned Mg_2Si is 0.78 GPa, which is slightly lower than that (0.93 GPa) under pure shear load. This suggests that compression plays a minor role in the mechanical strength of nanotwinned Mg_2Si. However, we find that compression plays an essential role in determining the strength of flawless Mg_2Si, since under biaxial shear load the mechanical strength of Mg_2Si along (1-1-1)[-11-2] is 3.88 GPa, much lower than its ideal shear strength of 6.88 GPa.

Among all the shear-stress – shear-strain relations (Fig. 1), the shear stress monotonically increases with the increasing shear strain. Beyond the maximum shear stress point, the shear stress gradually decreases, suggesting a typical structural softening.

To character this structural softening and understand the deformation mechanism, we examined the atomic configurations and bond changes of single crystal Mg_2Si against shear strain along the (1-1-1)[-11-2] system, as shown in Fig. 2. Under pure shear load, the Mg—Si framework uniformly resists the deformation (Fig. 2(a)) as the shear strain increases to 0.21 corresponding to the ideal strength. The Mg_1—Si_1 bond is shrunk from 2.75 to 2.65 Å with a shrinking ratio of 3.6%, while the Mg_2—Si_1 bond is stretched from 2.75 to 2.84 Å with a stretching ratio of 3.3% (Fig. 2(c)). As the shear strain increases to 0.41, the Mg—Si framework was further sheared to accommodate the

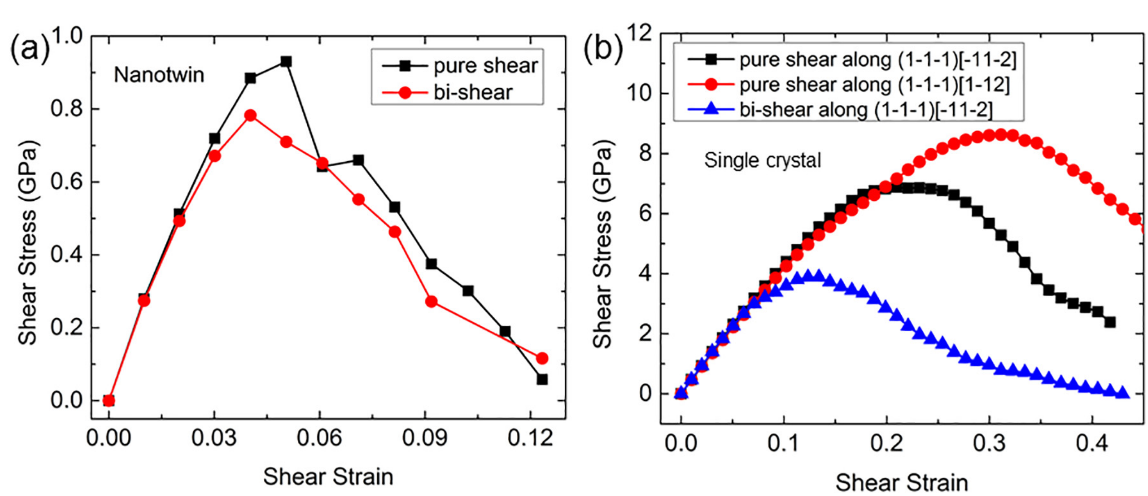

Fig. 1. Computed shear-stress – shear-strain relations of (a) nanotwinned Mg_2Si, as well as a comparison with that of (b) single crystalline Mg_2Si under pure shear and bi-shear loads.

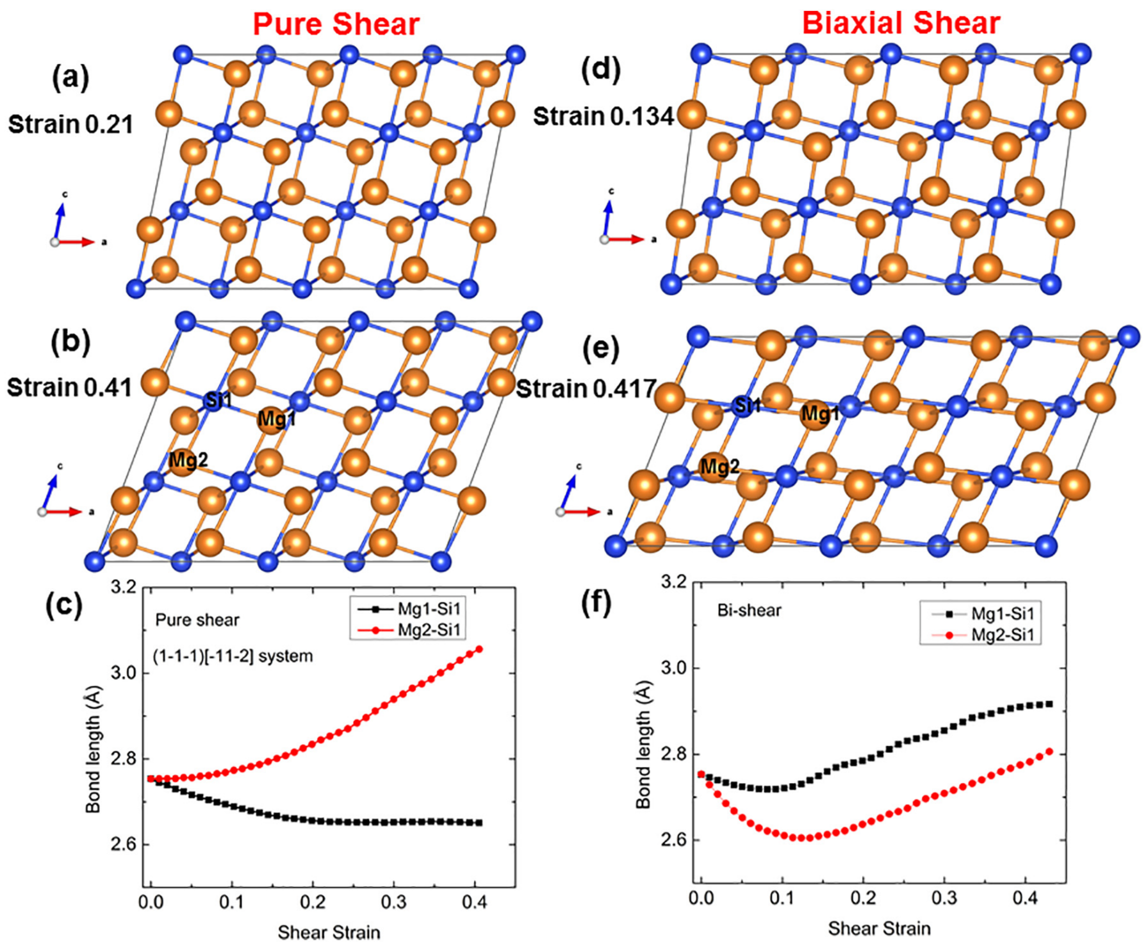

Fig. 2. Deformation mechanism of single crystal Mg_2Si under pure shear and biaxial shear loads along the (1-1-1)[-11-2] system. (a) Atomic structure at 0.21 shear strain under pure shear load, (b) Atomic structure at 0.41 shear strain under pure shear load, (c) The Mg_1—Si_1 and Mg_2—Si_1 bond lengths as a function of shear strain under pure shear load. (d) Atomic structure at 0.134 shear strain under biaxial shear load, (e) Atomic structure at 0.417 shear strain under biaxial shear load, (f) The Mg1-Si1 and Mg2-Si1 bond lengths as a function of shear strain under biaxial shear load.

external deformation (Fig. 2(b). The Mg_1—Si_1 bond length remains unchanged, while the Mg_2—Si_1 bond is rapidly stretched to 3.06 Å, leading to the softened Mg_2—Si_1 bond. This clearly shows that the Mg_2—Si_1 bond is responsible for the structural softening, giving rise to the gradually decreasing shear stress, as shown in Fig. 1(b).

Under biaxial shear load, as the shear strain increases to 0.134, the Mg—Si framework is compacted to resist the external deformation (Fig. 2(d)). At 0.417 shear strain, the structure is largely expanded along the *a* axis but is nearly unchanged along the *c* axis (Fig. 2(e)). To explain this deformation mode, we extracted the bond length changes, as shown in Fig. 2(f). The Mg_1—Si_1 bond is slightly shrunk and then rapidly stretched. At 0.417 shear strain, the Mg_1—Si_1 bond is stretched from 2.75 to 2.92 Å. This Mg_1—Si_1 bond stretching leads to the bond softening, resulting in the Mg—Si framework softening, and hence decreasing the ideal shear strength. In addition, the Mg_2—Si_1—Mg_1 bond angle rapidly increases from 70.5° to 108.2° at 0.417 shear strain. The largely increased Mg_2—Si_1—Mg_1 bond angle and stretched Mg1-Si1 bond length well explain the remarkably structural expansion along the *a* axis (Fig. 2(d)–(e)). The Mg_2—Si bond is rapidly shrunk to 2.61 Å with a shrinking ratio of 5.1% as the shear strain increases to 0.134 (Figure (f)). However, with further increasing shear strain, the Mg_2—Si_1 bond starts to stretch, recovering to its original length at 0.387 shear strain. At 0.417 shear strain, the Mg_2—Si_1 bond is only slightly stretched to 2.80 Å, slightly longer than its equilibrium bond length of 2.75 Å. Thus, the compression along the *c* axis suppresses the Mg_2—Si_1 bond stretching, leading to the nearly unchanged structural size along the *c* axis (Fig. 2(d)–(e)).

Moreover, we also extract the atomic configuration of Mg_2Si along the opposite direction (1-1-1) [1–12] and find that the Mg_1—Si_1 bond deformation dominants the structural softening, as shown in Fig. S5.

To understand the underlying nanotwin-induced softening mechanism, we extract the atomic configurations and bond length changes of nanotwinned Mg_2Si, as shown in Fig. 3. In the nanotwinned structure (Fig. 3(a)), the upper half part corresponds to the (1-1-1) [1–12] system, while the lower half part corresponds to the (1-1-1)[-11-2] system. The TB lies along the {1-1-1} plane with Si atoms locating in the TB. In the vicinity of TB, the Mg—Si bond length, such as Mg_1—Si_2 and Mg_3—Si_3, is 2.88 Å. This length is much higher than that (2.75 Å) of the Mg—Si bond in the crystal of Mg_2Si, suggesting that the rigidity of Mg—Si bond in the TB is much weaker than that in the single crystal. In addition, a new Mg—Mg bond (Mg_1—Mg_2) forms with the length of 2.55 Å. As the shear strain increases to 0.05, the Mg—Si framework in the TB is distorted accommodating the shear deformation due to the anti-symmetry of the nanotwinned structure (Fig. 3(b)). The Mg_1—Si_1 bond is largely stretched from 2.88 to 3.08 Å with a stretching ratio of 6.9%, while other bonds in the TB remain unchanged (Fig. 3(d)). This suggests that the Mg_1—Si_1 bond in the lower half part of the nanotwinned structure rapidly softens with the increasing shear strain. It is noted here that the Mg_1—Si_1 bond in the (1-1-1)[-11-2] system softens, rather than the Mg_2—Si_1 bond in the (1-1-1) [1–12] system. This is because the (1-1-1) [1–12] system is much stronger than the (1-1-1)[-11-2] system in resisting the deformation, as shown in Fig. 1 (b). At 0.06 shear strain, the Mg—Sb_1 bond sharply increases to 5.19 Å, representing the bond breakage. This leads to the structural

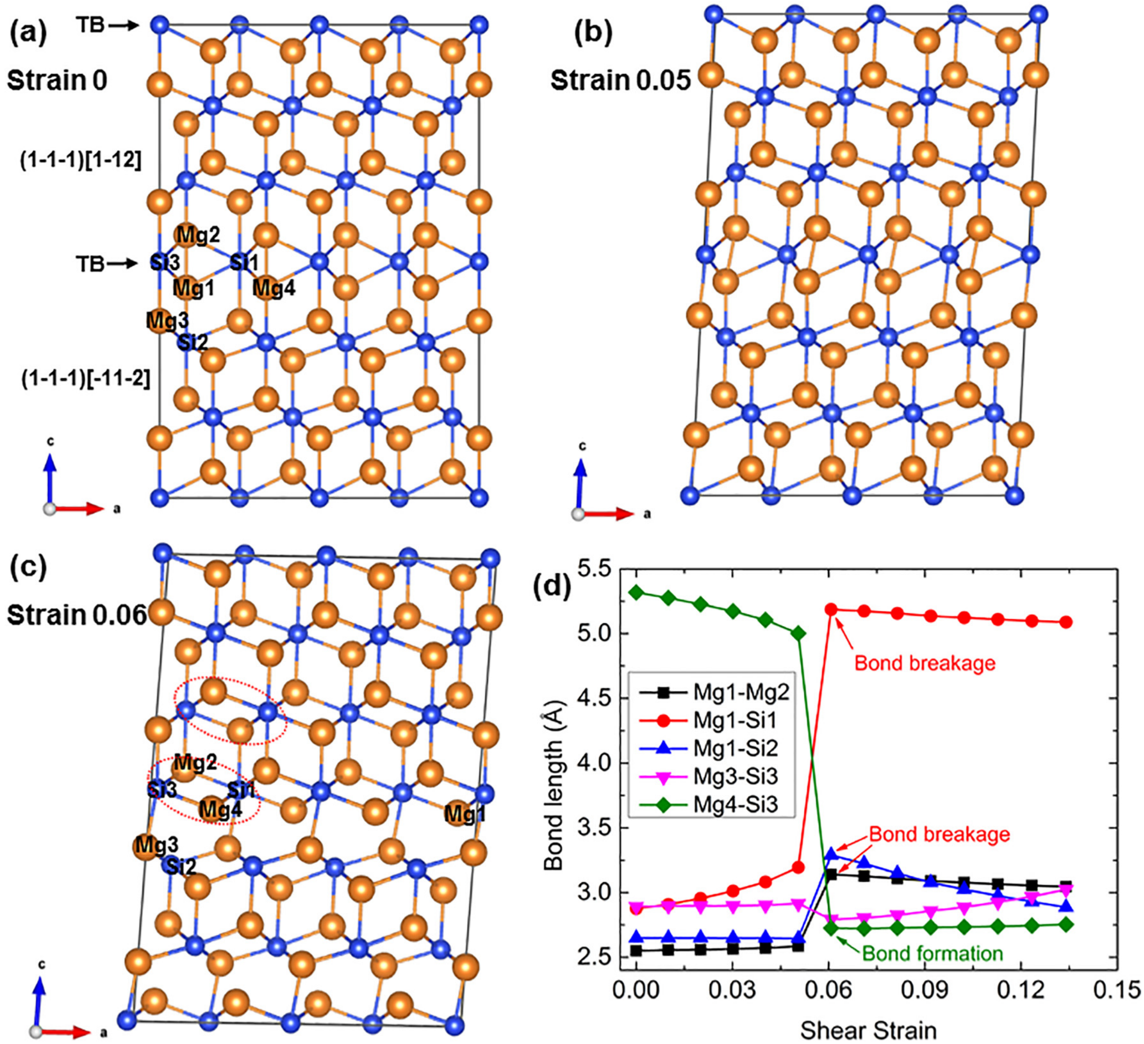

Fig. 3. Deformation mechanism of nanotwinned Mg_2Si under pure shear load. (a) Intact atomic structure, (b) Atomic structure at 0.05 shear strain, which corresponding to the maximum shear strength, (c) Atomic structure at 0.06 shear strain, (d) The typical bond lengths (Mg_1—Mg_2, Mg_1—Si1, Mg_1—Si_2, Mg_3—Si_3, and Mg_4—Si_3) against shear strain. The dashed red line highlights the same Mg—Sb framework in the TB and (1-1-1) [1–12] system. (For interpretation of the references to colour in this figure legend, the reader is referred to the web version of this article.)

rearrangement in the TB. For example, The Mg_1—Mg_2 bond increases from 2.58 to 3.14 Å. The Mg_1—Si_2 length increases from 2.65 to 3.29 Å, breaking this bond. While a new Mg_4—Si_3 bond forms with the length changes from 5.0 to 2.72 Å. This structural rearrangement forms a stable Mg—Sb framework, which is the same with that in the (1-1-1) [1–12] system, as highlighted in Fig. 3(c). The Mg_3—Si_3 bond length slightly decreases from 2.91 to 2.80 Å, indicating that the Mg_3—Si_3 is still linked with each other. Thus, this structural rearrangement doesn't collapse the structure. With the further increasing shear strain, the softening of the Mg_3—Si_3 bond leads to the structural softening (Fig. 3(d)) and the reduced shear stress, as shown in Fig. 1(a). In addition, the atomic configurations under biaxial shear load (Fig. S6) clearly show that compression along the *c* axis has little influence on the deformation mechanism of nanotwinned Mg_2Si.

Herein, we found that nanotwins significantly reduce the strength and elastic modulus of Mg_2Si, which indicates that nanotwins would be expected to play a significant role in modifying the phonon transport and hence TE properties of Mg_2Si. This requires a comprehensive study in the future.

Substitution of Si by Sn to form $Mg_2Si_{1-x}Sn_x$ alloys is essential to improve the TE properties of Mg_2Si [3]. Here, we investigated the influence of Sn dopant on mechanical properties of Mg_2Si, as shown in Fig. S7. We found that $Mg_2Si_{0.5}Sn_{0.5}$ have inferior mechanical properties than Mg_2Si (Fig. S7(a)). The elastic modulus and ideal shear strength of $Mg_2Si_{0.5}Sn_{0.5}$ are 32.0 GPa and 4.42 GPa, respectively. They are much lower than those (46.4 GPa and 6.88 GPa) of Mg_2Si. To understand the deformation mechanism of $Mg_2Si_{0.5}Sn_{0.5}$, we extracted the atomic configurations and bond response (Fig. S7(b)–(d)). Mg_2—Sn_1 and Mg_3—Si_1 bonds are slightly stretched while Mg_1—Sn_1 and Mg_4—Si_1 bonds are slightly shrunk resisting the deformation until the 0.221 shear strain, before failure. At the failure strain of 0.232, the Mg_1—Sn_1 and Mg_2—Sn_1 bonds break, destructing the structure and leading to the failure of $Mg_2Si_{0.5}Sn_{0.5}$. While the Mg_3—Si_1 and Mg_4—Si_1 bonds are still held together. This indicates that the rigidity of the Mg—Sn bond is weaker than that of the Mg—Si bond. Thus, substitution of Si by Sn softens the rigidity of Mg—Si framework, leading to the inferior mechanical behavior of $Mg_2Si_{0.5}Sn_{0.5}$ than Mg_2Si (Fig. S7(a)).

In summary, we apply *ab-initio* simulations to determine the role of nanotwins on the intrinsic shear strength and the deformation mode of TE semiconductor Mg_2Si. We found that nanotwinning softens Mg_2Si. Mg—Si bond is expanded in TB and thus softened to accommodate the structural mismatch, weakening TB rigidity and hence leading to a low ideal shear strength. Our work showed that grain boundary engineering strategy is further required to improve the mechanical properties of nanotwinned Mg_2Si for its engineering applications.

This work is partially supported by NSF of China under No. 51772231, the 111 Project of China under Project no. B07040. Q.A. was supported by the National Science Foundation CMMI program under grant no. 1727428. S.M. was thankful for the support by Act 211 Government of the Russian Federation, under No. 02.A03.21.0011 and by the Supercomputer Simulation Laboratory of South Ural State University [26].

Appendix A. Supplementary data

The structural relaxation and mechanical loading method; Nanotwinned structure before relaxation and after relaxation; The neighbor structure of the Si atom at the TB; The stress tensor of nanotwinned Mg_2Si during pure shear process; Deformation mechanism of flawless Mg_2Si under pure shear load along the (1-1-1) [1–12] system; Deformation mechanism of nanotwinned Mg_2Si under biaxial shear load; Influence of Sn dopant on mechanical properties of Mg_2Si. Supplementary data associated with this article can be found in the online version, at doi: https://doi.org/10.1016/j.scriptamat.2018.08.002.

References

[1] G.J. Snyder, E.S. Toberer, Nat. Mater. 7 (2008) 105.
[2] J. He, T.M. Tritt, Science 357 (2017) 1369.
[3] W. Liu, X.J. Tan, K. Yin, H.J. Liu, X.F. Tang, J. Shi, Q.J. Zhang, C. Uher, Phys. Rev. Lett. 108 (2012) 166601.
[4] Q. Zhang, J. He, T.J. Zhu, S.N. Zhang, X.B. Zhao, T.M. Tritt, Appl. Phys. Lett. 93 (2008) 102109.
[5] J.H. Li, X.P. Li, B.W. Cai, C. Chen, Q. Zhang, Z.S. Zhao, L. Zhang, F.R. Yu, D.L. Yu, Y.J. Tian, B. Xu, J. Alloys Compd. 741 (2018) 1148.
[6] A. Usenko, D. Moskovskikh, A. Korotitskiy, M. Gorshenkov, E. Zakharova, A. Fedorov, Y. Parkhomenko, V. Khovaylo, Scr. Mater. 146 (2018) 295.
[7] D. Kato, K. Iwasaki, M. Yoshino, T. Yamada, T. Nagasaki, J. Solid State Chem. 258 (2018) 93.
[8] S. Nakamura, Y. Mori, K. Takarabe, Phys. Status Solidi C 10 (2013) 1145.
[9] L. Lu, Y.F. Shen, X.H. Chen, L.H. Qian, K. Lu, Science 304 (2004) 422.
[10] Q. An, W.A. Goddard, K.Y. Xie, G.D. Sim, K.J. Hemker, T. Munhollon, M.F. Toksoy, R.A. Haber, Nano Lett. 16 (2016) 7573.
[11] Q. Huang, D.L. Yu, B. Xu, W.T. Hu, Y.M. Ma, Y.B. Wang, Z.S. Zhao, B. Wen, J.L. He, Z.Y. Liu, Y.J. Tian, Nature 510 (2014) 250.
[12] Y.J. Tian, B. Xu, D.L. Yu, Y.M. Ma, Y.B. Wang, Y.B. Jiang, W.T. Hu, C.C. Tang, Y.F. Gao, K. Luo, Z.S. Zhao, L.M. Wang, B. Wen, J.L. He, Z.Y. Liu, Nature 493 (2013) 385.
[13] G.D. Li, U. Aydemir, S.I. Morozov, M. Wood, Q. An, P.C. Zhai, Q.J. Zhang, W.A. Goddard, G.J. Snyder, Phys. Rev. Lett. 119 (2017), 085501. .
[14] G.D. Li, S.I. Morozov, Q.J. Zhang, Q. An, P.C. Zhai, G.J. Snyder, Phys. Rev. Lett. 119 (2017) 215503.
[15] J.I. Jang, J.E. Lee, B.S. Kim, S.D. Park, H.S. Lee, RSC Adv. 7 (2017) 21671.
[16] G. Kresse, J. Furthmuller, Comput. Mater. Sci. 6 (1996) 15.
[17] G. Kresse, J. Furthmuller, Phys. Rev. B 54 (1996) 11169.
[18] G. Kresse, D. Joubert, Phys. Rev. B 59 (1999) 1758.
[19] J. Perdew, K. Burke, M. Ernzerhof, Phys. Rev. Lett. 77 (1996) 3865.
[20] G. Li, U. Aydemir, S.I. Morozov, S.A. Miller, Q. An, W.A. Goddard, P. Zhai, Q. Zhang, G.J. Snyder, Acta Mater. 149 (2018) 341.
[21] G. Li, U. Aydemir, B. Duan, M.T. Agne, H. Wang, M. Wood, Q. Zhang, P. Zhai, W.A. Goddard III, G.J. Snyder, ACS Appl. Mater. Interfaces 9 (2017) 40488.
[22] G. Li, Q. An, W. Li, W.A. Goddard, P. Zhai, Q. Zhang, G.J. Snyder, Chem. Mater. 27 (2015) 6329.
[23] T.-W. Fan, J.-L. Ke, L. Fu, B.-Y. Tang, L.-M. Peng, W.-J. Ding, J. Mag. Alloys. 1 (2013) 163.
[24] D.H. Chung, Philos. Mag. 8 (1963) 833.
[25] Q. An, W.A. Goddard, Appl. Phys. Lett. 110 (2017) 111902.
[26] P.S. Kostenetskiy, A.Y. Safonov, Proceedings of the 10th Annual International Scientific Conference on Parallel Computing Technologies (Arkhangelsk, Russia), 2016.